Measurement of stoichiometry and turnover in single, functioning membrane protein complexes

Leake *et al.*

Supplementary Information

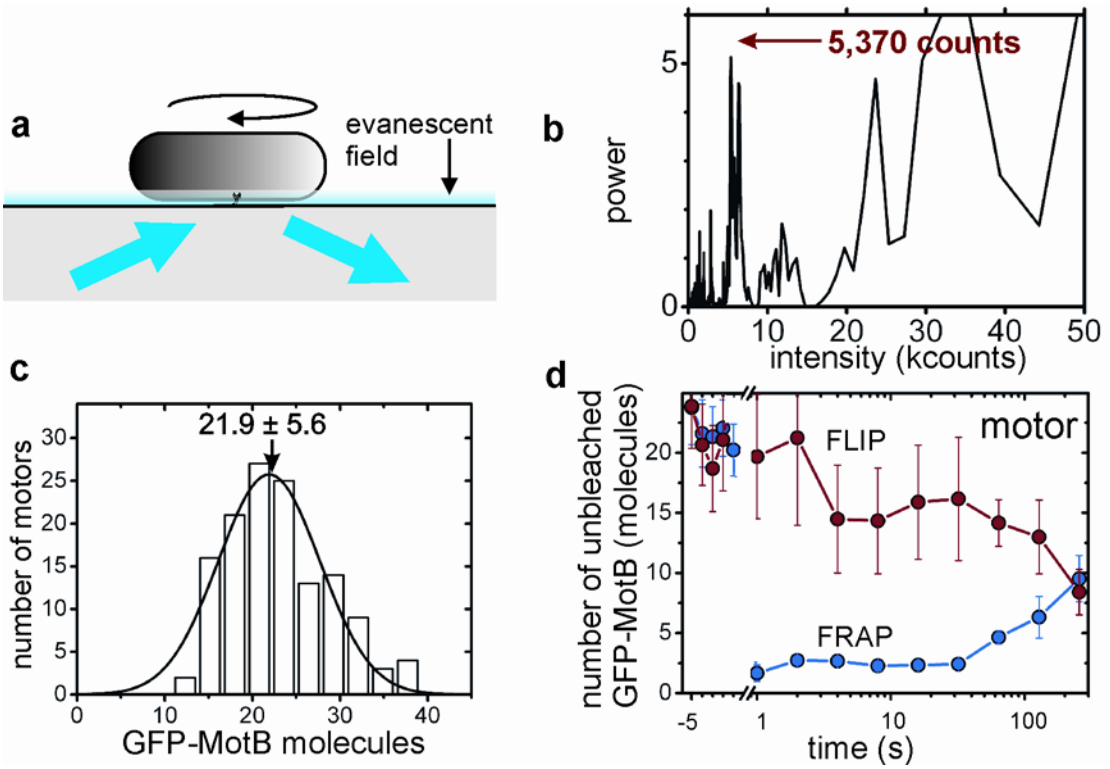

Supplementary Figure 1 Summary figure showing main results. a TIRF imaging was performed on GFP-MotB cells. **b** Continuous photobleaching could be resolved into ~integer multiples of a unitary step of size ~5,400 counts associated with a single GFP molecule. **c** Estimations were made for number of GFP-MotB present at the motor based on step-wise photobleaching of GFP. **d** FLIP and FRAP after focussed laser bleaching indicate rapid active turnover of GFP-MotB in the functional motor complex.

Supplementary Methods 1

***E. coli* strain construction**. A construct containing 500bp upstream of and including the first 28 codons of *motB* (encompassing the putative membrane-targeting sequence), followed by *egfp* and then the first 500bp of *motB*, was generated by overlap extension PCR[28] and cloned into pKO3. This was sequenced and inserted into the *E. coli* RP437 chromosome by allelic exchange[29].

Measurement of GFP-MotB expression levels. We measured expression levels of MotB and GFP-MotB in wild-type (RP437) and *gfp-motB* strains respectively using quantitative western blotting (Supplementary Figure 2). We grew cells to OD_{600}=0.8 and centrifuged 1 ml of cells and resuspended the pellet in 50µl of SDS-PAGE buffer. Cell lysates were subjected to SDS-PAGE, blotted onto nitrocellulose membranes and hybridized with an anti-MotB antibody (donation of David Blair, University of Utah,

USA) followed by anti-rabbit HRP. We scanned the exposed nitrocellulose membranes and calculated the total pixel intensity within each discrete band (ImageQuant, Molecular Dynamics). The total intensity for the RP437 wild-type strain divided by that for the *gfp-motB* strain was 0.93±0.14 (mean±s.e.m., n=6), consistent with the *gfp-motB* gene having similar expression levels to wild-type *motB*.

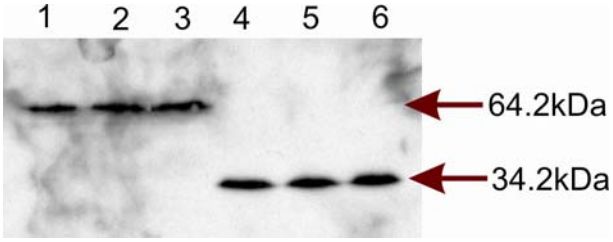

Supplementary Figure 2 Anti-MotB western blot of cell lysates. Cell lysates from the *gfp-motB* strain (lanes 1-3) and RP437 parental strain (lanes 4-6), each from separate cultures. Lysates were subjected to SDS-PAGE, blotted on a nitrocellulose membrane and probed with 1:1000 dilution of primary antibody (anti-MotB antibody) followed by anti-rabbit-HRP. The respective molecular weights of GFP-MotB and MotB are indicated (arrows).

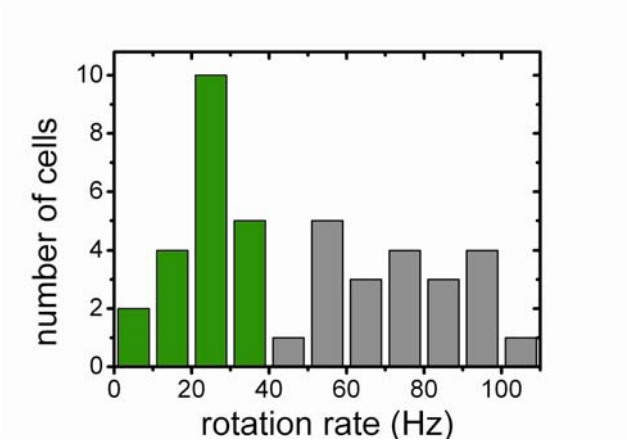

Supplementary Figure 3 Rotation rates of wild-type and GFP-MotB motors. We attached polystyrene beads of diameter 0.75 μm to sticky flagellar filaments and measured rotation rates with back-focal-plane interferometry as described[17]. For each cell we calculated the average speed over an interval of 5 s. Average speeds are binned and separate histograms plotted for *gfp-motB* (green) and wild-type (RP437, grey) strains. Mean ± s.d. for GFP-MotB and wild-type motors were 24 ± 16 Hz and 75 ± 10 Hz respectively. We measured 21 cells of each strain.

Cell preparation for microscopy. Cells were grown in tryptone broth (TB) with shaking at 30 ºC to OD_{600} = 0.8, resuspended in motility buffer (10 mM potassium phosphate, 0.1 mM EDTA, pH 7.0) or TB buffer (10% TB in motility buffer), flagellar filaments sheared[30] and cells incubated with anti-FliC antibody for 20 min. Where required chloramphenicol (50μg/ml) was added to suppress new protein synthesis 20 min prior to shearing and experiments carried out in CM buffer (50μg/ml chloramphenicol in motility buffer). Cells were injected into a ~5 μl flow-cell for tethered and stuck cell assays, with uncoated or polylysine-coated glass coverslips respectively as the lower surface. Cells were allowed to settle for 10 min, washed with excess motility, CM or TB buffer as appropriate, incubated with a 0.1 % suspension of 202nm diameter latex microspheres (Polysciences, Germany) for 2 min to mark the coverslip and washed with excess buffer.

Supplementary Note 1

Estimating the total number of motors per cell. We modelled the cell as a cylinder of length 2 μm and diameter 1 μm with hemispherical end-caps. We estimated that approximately one sixth of the surface is within 100 nm of the coverslip and thus within the TIRF illumination field. Thus the average of 1.0 ± 0.2 (mean ± s.e.m., n=63) motors per cell visible in TIRF images of stuck cells corresponds to 6.0 ± 1.2 motors in total, consistent with independent estimates of the total number of motors per cell[19].

Supplementary Methods 2

Separating motor and background components of fluorescence intensity. We read image files into custom-written analysis software (LabView 7.1, National Instruments, Austin, TX). We measured lateral sample drift by comparing time-stamped pre- and post-photobleach brightfield images (typically <400 nm per hour), applying a correction to all subsequent image frames by linear interpolation with time. Images of stuck cells showed bright spots with radially symmetric, approximately Gaussian, intensity profiles. The width of these spots was ~300 nm, consistent with a ring of GFP-MotB molecules bordering a rotor of diameter ~50 nm convoluted by the microscope point-spread-function. We calculated a fluorescence-intensity centroid for each putative motor spot. We made an initial estimate based on the centre of rotation of the cell body in the corresponding brightfield image, or on the peak pixel intensity of a given fluorescent spot, for the tethered and stuck cells respectively. We defined an 8x8 pixel (400x400nm) region of interest (ROI) centred on the initial motor centroid and separated motor and non-motor contributions to the total intensity within the ROI as follows:

1. We applied a circular motor mask of diameter 240 nm to the ROI, centred on the current motor centroid.

2. We multiplied pixel intensities within the motor mask by a radially symmetrical 2-dimensional Gaussian mask of fixed half-width (s.d.) 150 nm, and generated a revised estimate for motor centroid weighted by this mask[31].

3. We iterated steps 1 and 2 either 10 times or until the motor mask began clipping the side of the original ROI, generally resulting in a final centroid precision of ~5 nm.

4. We defined the total background intensity as the mean pixel intensity within the ROI but external to the final motor mask. We defined the motor intensity as the sum of all pixel values within the motor mask after subtraction of the total background intensity from each pixel value. For ROIs with no motor spot, we defined the total background intensity as the mean intensity of all pixels within the ROI.

5. We defined the instrumental component of background (the intensity not associated with cells) as the mean pixel intensity in a 400x400 nm ROI containing no cells.

We performed steps 1-5 separately for each image.

6. We defined the cell autofluorescence component of background as the mean pixel intensity within 32 400x400 nm ROIs from separate cells of the wild-type strain, RP437, containing no GFP.

7. We defined the membrane component of background (due to a diffusing pool of GFP-MotB) for each image as the total background intensity minus the instrumental component (step 5) and the autofluorescence component (step 6).

The average photobleach traces during continuous TIRF excitation for all cellular components are shown in Supplementary Fig. 4. The autofluorescence (Supplementary Fig. 4a) and total motor components (Supplementary Fig. 4b) were fitted by single exponential decays with bleach time constants 62 ± 1 s and 44 ± 1 s

respectively (mean ± s.e.m., n=32 and 134). The membrane component when measured in the presence of a motor in the ROI could not be modelled adequately by a single exponential decay (Supplementary Fig. 4e). However, the membrane component measured in the absence of a motor in the ROI could be fitted well by with a single exponential decay bleach of time constant 269 ± 8 s (Supplementary Fig. 4f). Possible reasons for the difference between membrane component traces in ROIs with and without motors follow from the calculation of the membrane component as a relatively small difference between two larger, separate, noisy measurements of total and autofluorescence components, and may include systematic errors in separation of the motor component from background that might be insignificant relative to motor component but significant relative to the membrane component; the apparent differences compared to measurements made in the presence of a motor may be attributable to the relatively high noise observed for both traces. We attribute the large difference between photobleaching rates of motor and membrane GFP components to diffusive mixing with unbleached GFP from outside the TIRF illumination region.

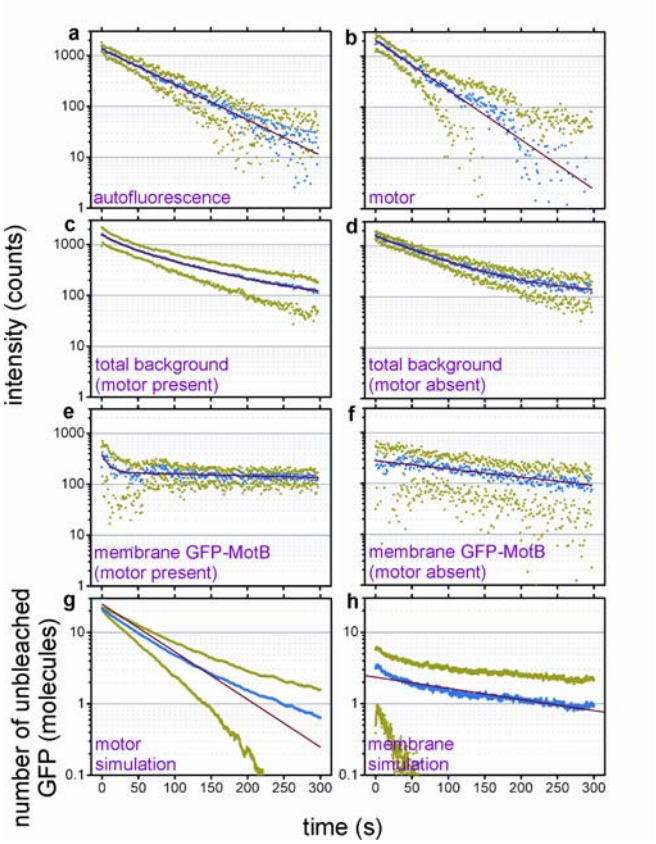

Supplementary Figure 4 Average continuous TIRF photobleach traces. Intensities (blue) are averages of data from 27-134 ROIs, with units of (intensity per pixel) for all traces except **b,** where the total motor intensity divided by 50 was chosen to allow use of a single intensity scale. **a**, Autofluorescence, from the parental non-GFP strain (n=32, single exponential decay, bleach time 62 s). **b**-**f**, GFP-MotB strain. **b,** motor component (n=134, single exponential decay, bleach time 44 s). **c, d,** Total background components in the presence (**c**, n=134, double exponential fit, bleach times 57 s and 274 s), and absence (**d,** n=27, double exponential fit, bleach times 68 s and 262 s) of a motor in the ROI motor. **e, f,** Membrane GFP-MotB component in the presence (**e,** n=134, double exponential fit) and absence (**f,** n=27, single exponential decay, bleach time 269 s) of a motor in the ROI. s.d. error (green) and fit (red) are shown for each trace. Average traces from simulations of the TIRF bleach (Supplementary Methods 7) gave similar results for the motor component (**g,** n=500, single exponential decay, bleach time 59 s, expressed as number of unbleached GFP molecules) and the membrane component (**h,** n=500, single exponential decay, bleach time 274 s, expressed as number of unbleached GFP molecules μm^{-2}).

Supplementary Methods 3

Counting fluorescent molecules. Tests using simulated bleach traces with similar noise levels to experimental traces indicated that separation into motor and background components (Supplementary Methods 2) recovered the exponential bleach traces without introducing significant errors. However, separation also generated artifactual fluctuations in intensity at roughly the same level as the noise in the original traces. Since putative single GFP bleach events were of a similar size to noise this made the approach for the detecting single-molecule GFP bleaching in either separated component unreliable. Therefore, we detected step-wise photobleaching from the total intensity signal (minus instrumental background), as follows:

We filtered each photobleach intensity trace using an edge-preserving Chung-Kennedy algorithm consisting of two adjacent running windows whose output was the mean from the window possessing the smallest variance[22, 32-33]. We then calculated all pairwise differences in the filtered intensity trajectories $I(t)$:

$$\Delta I_{ij} = I(t_i) - I(t_j)$$

for all data pairs for which the time $t_i > t_j$. The distribution of these pairwise differences (Pairwise Difference Distribution Function, PDDF) was calculated using 2,000 bins per trajectory and normalized by the total number of pairwise differences, $n(n - 1)/2$, where n is the number of datapoints in each trace[34]. We then calculated the single-sided power spectrum from each pairwise displacement histogram. Peak detection in the power spectrum was automated using commercial code (LabView 7.1, National Instruments, Austin, TX) with the unitary step peak taken as that detected at the highest spatial frequency in each trace[23], taking a peak detection threshold as four standard deviations above the high spatial frequency noise floor (defined as the standard deviation of the power spectrum signal between S_{fmax} and $S_{fmax}/2$, where S_{fmax} is the maximum spatial frequency for the power spectrum) equivalent to a probability confidence level of $P<0.001$. The corresponding value of spatial frequency was inverted to give the characteristic "unitary step size" in terms of intensity counts. The total number of steps was estimated as the initial motor intensity estimated from the exponential fit to the motor-only component I_0^m divided by the unitary step size I_{GFP} for each individual bleach trace.

Supplementary Figs. 5a and 5b show distributions of I_{GFP} and I_0^m respectively, for 134 traces from different cells, with Supplementary Fig. 5c our estimate for the total number of GFP-MotB molecules per motor by dividing I_0^m by I_{GFP} for each trace.

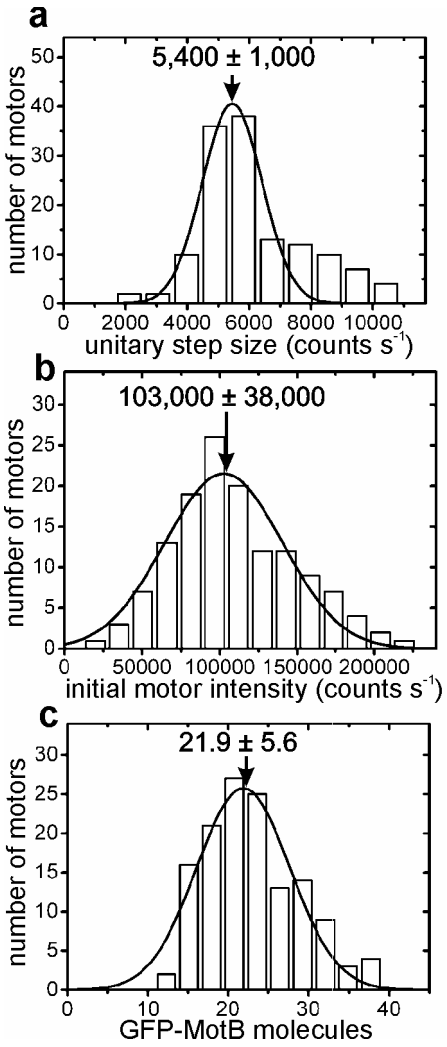

Supplementary Figure 5 Histograms for pooled tethered and stuck cell data (134 bleaches). a, Unitary step size, **b,** initial motor spot intensity I_0^m, **c,** estimated number of GFP-MotB molecules per motor. The peak of the histogram in **c** and the ratio of the peaks in **a** and **b** give estimates for the average number of GFP-MotB molecules per motor. Gaussian fits are shown with mean ± s.d. indicated.

Supplementary Methods 4

Pre-bleaching membrane fluorescence to improve step detection efficiency. To improve the clarity of the photobleach steps in the raw intensity signal we experimented with a modified bleaching protocol consisting of the following:

1. Obtain 10 consecutive TIRF image frames at 10 Hz sampling rate for a stuck cell at an intensity of ~250 W cm^{-2} (i.e. sampled ten times faster than for the usual 1 Hz protocol and with a tenfold greater excitation intensity, therefore roughly the same anticipated image intensity in terms of counts $pixel^{-1}$ $frame^{-1}$).
2. Perform a focussed laser bleach at an intensity of ~10 kW cm^{-2} , typically for 0.5-2.0 s.
3. Observe consecutive TIRF image frames at 10 Hz sampling as in (1), for a further ~30 s.

During the focussed laser pre-bleach, fluorescence from beyond the ~1 μm region of the beam focus (Supplementary Figs. 6a-c middle panels) indicated light scattering within the cell transferring some proportion of excitation light beyond the original laser focus. Thus the effect of the focussed laser spot pre-bleach was to reduce the background fluorescence components considerably and to reduce the motor fluorescence component somewhat less (compare images before pre-bleach, Supplementary Figs. 6a-c left panels with those after, Supplementary Figs. 6a-c right panels; see also Supplementary Fig. 6d). Photobleaching steps in the motor fluorescence component could be identified directly in TIRF images obtained after the pre-bleach, due to the reduced background (Supplementary Figs. 6e-i). These steps were detected automatically by an algorithm as follows. We filtered each motor intensity trace using an edge-preserving Chung-Kennedy (C-K) algorithm consisting of two adjacent running windows whose output was the mean from the window possessing the smallest variance[22, 32-33]. Step events in the data were detected by applying a single-tailed Student *t*-test between the sample means from the two Chung-Kennedy windows, with the criterion for acceptance of a true step being $P<0.001$. We defined the step size as the difference between the sample means of the windows either side of the position of each detected step. The advantage of this method compared to the PDDF method (Supplementary Methods 3) was that the step size, confidence level and time were obtained directly for each individual step. Typical values for step sizes were ~integer multiples of a value in the range 4,500-6,500 count s^{-1}. This was consistent with the distribution of unitary steps obtained from PDDF analysis of the 1 Hz sampling protocol (Supplementary Fig. 5c), which had a mean of 5,400 ± 1,000 counts s^{-1}. Although not a replacement method for estimating number of GFP-MotB molecules in the motor, since an unknown number are bleached during the focussed laser spot bleach, this result corroborates our estimate of the unitary step size corresponding to bleaching of one GFP molecule.

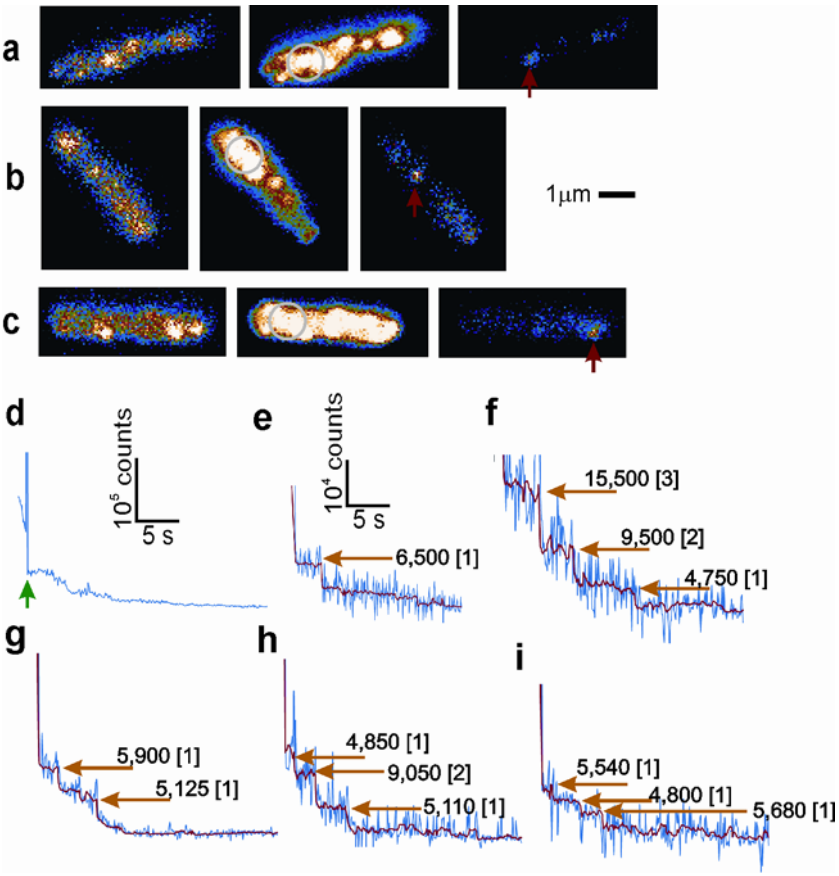

Supplementary Figure 6 Less noisy steps obtained by pre-bleaching. **a-c,** Three example cells: left panel=pre-bleach, middle panel=focussed laser bleach (circle=extent of original laser focus width), right panel=immediately post-bleach. Position of motor under observation indicated (red arrow). **d,** A typical trajectory of the motor component of fluorescence intensity, with the focussed laser spot pre-bleach indicated (green arrow). **e-i,** Expanded data from several motors in the post-bleach region showing raw motor intensity (blue), Chung-Kennedy filtered motor intensity (red) and position of detected steps (orange arrow) with the measured step size for each indicated along with [equivalent corresponding number of bleached GFP molecules to the nearest integer] based on a unitary step size of ~5,400 counts s^{-1}. The traces in **h** and **i** are also shown in Fig. 2e.

Supplementary Methods 5

Fluorescence microscopy. We used a home-built inverted fluorescence microscope with a x100 Plan Fluor 1.45 NA oil-immersion objective (Nikon UK Ltd., UK) and an xyz nanopositioning stage (E-503.00, Physik Instrumente, Germany). Brightfield used fiber-coupled tungsten-halogen illumination; laser excitation a fiber-coupled TEM00 plane-polarized multi-line argon-ion laser (Melles Griot, USA), filtered (laser-line, 488 nm), expanded x3 and focussed onto the back-focal-plane of the objective lens via a dichroic mirror (505 nm long-pass). Controlled lateral movement of the focus equated to rotation of the emergent angle from the objective allowing switching between epifluorescence and TIRF. The field width was ~60 μm, intensity ~25 W cm^{-2} (~1 kW cm^{-2} for immobilized GFP molecules, ~250 W cm^{-2} for particle tracking). A separately-shuttered excitation path allowed a proportion of the laser light to be focussed in the sample plane to a width ~1 μm, intensity ~35 kW cm^{-2}. Fluorescence emission was passed through the dichroic mirror, an emission filter (535 nm band-pass) and a notch rejection filter (488 nm), and imaged at ~50 nm per pixel in frame-transfer mode at 1 Hz (25 Hz for immobilized GFP molecules, 10 Hz for particle tracking) by a 128x128-pixel, cooled, back-thinned electron-multiplying charge-coupled-device camera (iXon DV860-BI, Andor Technology, UK).

The schematic for the custom-built TIRF microscope is shown in Supplementary Fig. 7a. Controlled lateral movements of lens L2 via a micrometer translation stage result in a change to the emergent angle θ of the beam from the objective lens into the sample. By replacing the sample with a glass prism in optical contact with the objective lens we were able to characterize the variation in θ as a function of L2 displacement from the optic axis (Supplementary Fig. 7b, zero displacement defined as on-axis epifluorescence). We then used the relation[35]:

$$d = \frac{\lambda}{4\pi\left(n_1^2 \sin(\theta)^2 - n_2^2\right)^{1/2}}$$

Here, d is the depth of penetration for the evanescent field for an excitation wavelength λ with the refractive indices n_1 and n_2 being for immersion oil (1.52) and water (1.33) respectively (Supplementary Fig. 7c). For TIRF microscopy measurements were generally performed with an L2 displacement of 2.5 mm, equivalent to $d = 97 \pm 11$ nm.

Image acquisition and Photobleaching. Mid cell-body height from the coverslip was measured for each cell and a video of brightfield images (40 ms exposure) recorded 100 nm above the coverslip. For TIRF bleaches, continuous excitation using TIRF was initiated by opening a mechanical shutter simultaneously with the start of fluorescence data acquisition. Images were sampled continuously for 300 s resulting in >90% photobleaching within range of the TIRF field ~100nm from the coverslip. Where required, widefield epifluorescence photobleaching was performed for a further 300 s. For slow recovery experiments, single exposures were taken in TIRF at intervals up to 90 min after TIRF or epifluorescence bleaching. For FRAP and "one-shot" FLIP experiments, single exposures were taken in TIRF at intervals up to 256 s after first acquiring 5 consecutive TIRF exposures then bleaching with the focussed laser for 0.5 s, centred either over a fluorescent spot of a putative motor (FRAP) or >1 μm distant from a motor (FLIP), using both stuck and tethered cells in CM buffer. "One-shot" FLIP differs from conventional FLIP[11], in that only a single photobleach

is used. Motor and membrane components were separated as described in the text for TIRF bleaches. Average curves were generated for FRAP and FLIP of both motor and membrane components, with all intensity components corrected for photobleaching during observation by multiplication with a cumulative factor $\exp(t_{total}/t_0)$ where t_{total} is the total accumulated time under TIRF observation and t_0 is the appropriate bleach time constant (Table 1). These were normalized to the average intensity component from the 5 pre-bleach exposures and multiplied by our estimate for number of GFP-MotB at the motor or in the membrane to generate curves for number of unbleached GFP-MotB vs time. A final brightfield video was taken to assess lateral drift and cell rotation speed. All experiments were performed at 23 ºC.

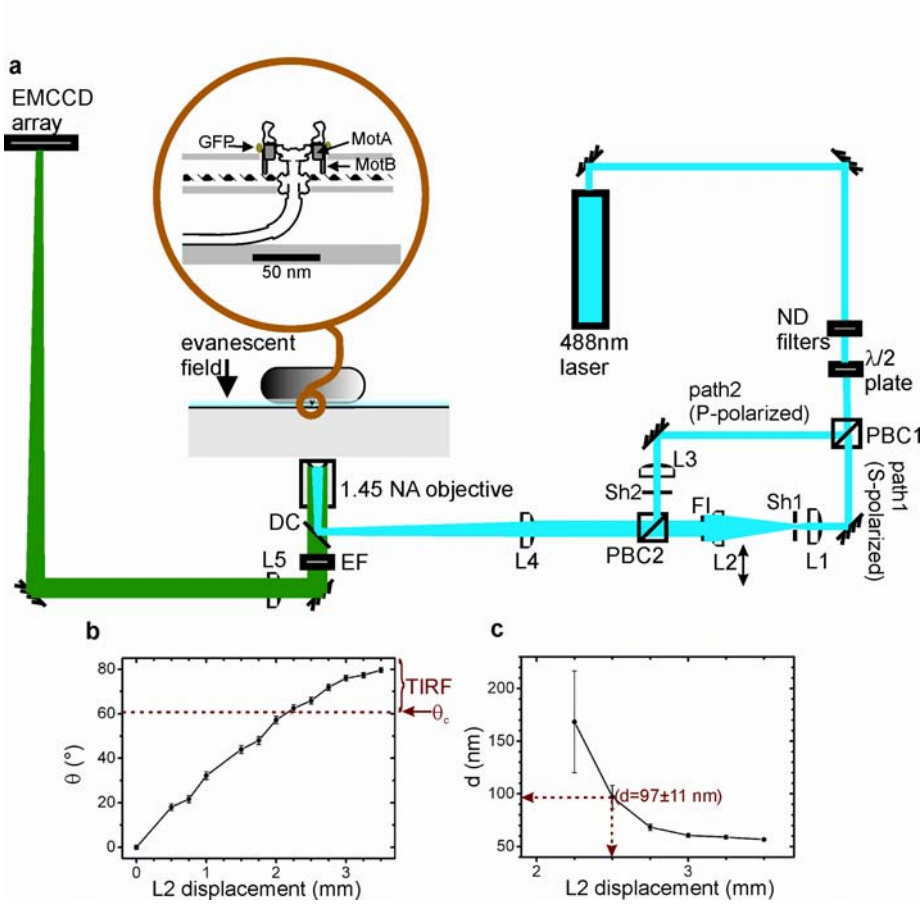

Supplementary Figure 7 TIRF penetration depth. **a,** Schematic of TIRF microscope (ND=neutral density filters, PBC=polarizing beam-cube, L=lens, DC=dichroic mirror, EF=emission filter,FI=field iris, Sh=shutter). **b,** Variation of emergent angle θ from objective lens with lens L2 displacement from the optic axis. **c,** Equivalent variation of depth of penetration *d* of the evanescent field.

Supplementary Methods 6

Estimating the diffusion coefficient 1: Comparison with Simulations. We simulated two-dimensional diffusion over the cell surface using custom-written software (MATLAB modified from ref. 26), modelling the cell as a cylinder of length 2 μm and diameter 1 μm capped with hemispherical ends. We assumed each cell contained ~200 GFP-MotB molecules in total (as per our experimental estimation), initially randomly distributed over the total surface area. We assigned a centre for the focussed laser bleach on the long-axis of the cell, either in the centre or displaced 0.5-1.0 μm from the centre towards one of the poles. We assumed the photobleach probability to be a symmetrical two-dimensional radial Gaussian of width ~1 μm, normalized to match the observed experimental intensity levels for the membrane component of GFP-MotB just after bleaching, and polled each molecule as to whether it was photobleached or not. In each subsequent small time interval Δt (100ms) after the bleach we assumed each molecule to move a small distance $(4D\Delta t)^{1/2}$ in a random direction in the membrane, where D was a trial two-dimensional diffusion coefficient. We tracked the positions of all molecules during time intervals over a range 1 to 256 s to match experimental data.

To calculate the predicted TIRF image intensity from the positions of fluorescent molecules in the membrane we performed the following procedure:

1. We assigned a brightness to each unbleached molecule equal to the TIRF evanescent field weighting function of $\exp(-z/d)$, where z was the relevant height of each molecule at a given time point and d was the characteristic 1/e field depth, 100 nm.
2. We approximated the intensity profile of each unbleached molecule by a symmetric two-dimensional Gaussian of width 240 nm. This ignores the effect of de-focussing on the point-spread-function, which in practice will be very small as all visible molecules are close to the focal plane defined by the coverslip and TIRF illumination field.
3. We then binned the final intensity patterns into a two-dimensional pixel grid (50x50 nm per pixel), with the contribution from each molecule given by the weighted intensity (from steps 1 and 2 above) at the centre of the pixel.
4. We also simulated the effects of dimerization on the GFP-MotB molecules, i.e. assuming ~100 diffusing particles of double the unitary intensity, which resulted in very similar average trajectories when normalized to the initial intensity.

Supplementary Fig. 8a shows a projection of intensities due to all fluorophores in the cell in a typical simulation, including step 2 above but with an infinite TIRF field depth (left panel) and the corresponding predicted TIRF image following steps 1-3 above (right panel).

We simulated several values of D in the range 0.125 to 16×10^{-3} $\mu m^2 s^{-1}$, calculating the average TIRF intensity patterns from 10 cells for each. We then analysed the averaged image for each value of D using the same method as for experimental focussed laser FRAP and FLIP data, to assess the predicted recovery or loss of fluorescence intensity following photobleaching. We compared these predictions with the membrane background component in experimental FRAP data for ROIs which contained no putative motor (Supplementary Fig. 8b). We obtained an estimate for D at each time point by linear interpolation, and took the average of these estimates as the final estimate of D, 0.0075 ± 0.0013 $\mu m^2 s^{-1}$ (mean ± s.d.).

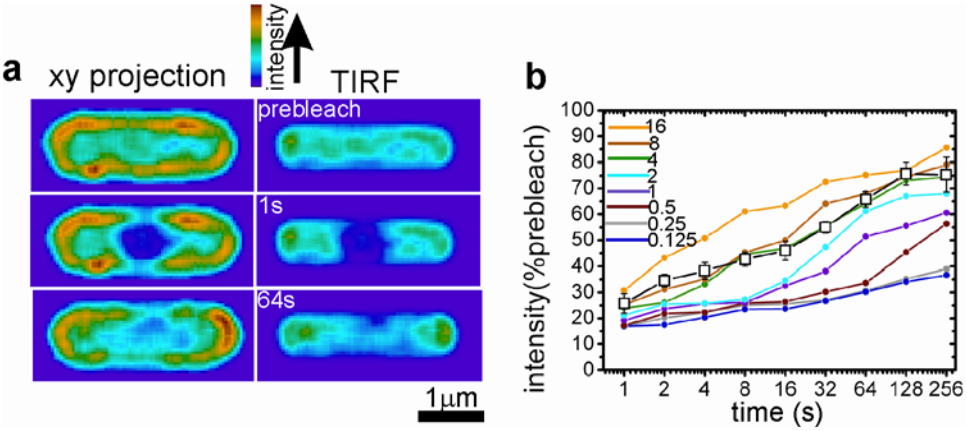

Supplementary Figure 8 Estimating the diffusion coefficient in the membrane by comparison with simulation. **a,** x-y projections and TIRF images (averages of 10 simulations) before and after focussed bleaching of the centre of the cell, D=1×10^{-3} μm^2 s^{-1}. **b,** Intensity in ROI centred on laser focus *vs.* time postbleach. Simulated traces (coloured) for values of D in range (0.125 to 16)×10^{-3} μm^2 s^{-1} and experimental data (black squares) from FRAP in non-motor regions (averaged from 8 GFP-MotB cells, error bars one s.d.)

Estimating the Diffusion Coefficient 2: Single-particle tracking. In experiments using the pre-bleach protocol (Supplementary Methods 4, Fig. 2d), the reduction in the background fluorescence was occasionally large enough to allow direct observation of dim, diffusing, fluorescent spots of width 250-300 nm in the post-bleach TIRF images (Supplementary Video 6), presumably in the cytoplasmic membrane. These spots were tracked frame-by-frame at 10 Hz, as follows:

1. The Gaussian-weighted intensity centroid of the spot was calculated for each frame (Supplementary Methods 2), with an estimated precision of ~50 nm. The starting point for the centroid algorithm in the first frame was determined by eye, in subsequent frames it was the centroid from the previous frame.
2. A spot in the $(i+1)^{th}$ frame was considered the same spot as that in the i^{th} frame provided:
   (a) Spot centroid(i+1) was within 300 nm (i.e approximately the spot width) of spot centroid(i).
   (b) Spot intensity(i+1) was within 75% of spot intensity(i).
   (c) Spot width(i+1) was within 30% of spot width(i).”
   (d) If >1 spots are present in the $(i+1)^{th}$ frame and the spots’ centroids are within 300 nm of each other then the tracking is terminated on the i^{th} frame.
   (e) If no spot is observed on the $(i+1)^{th}$ frame following observation of a spot in the i^{th} frame then tracking is terminated on the i^{th} frame.
3. Spot intensities (defined in the same way as motor intensity components, Supplementary Methods 2) and centroids were recorded as a function of time for each tracked spot (Supplementary Figs. 9a, b).

The mean end-to-end distance (r) covered in a time interval τ by a particle diffusing in 2 dimensions is given by $\langle r^2 \rangle = 4D\tau$. Supplementary Fig. 9c (left panel) shows

$\langle r^2 \rangle$ *vs* τ for the same spots as Supplementary Figs. 9a, b for all continuous, non-overlapping intervals of duration τ. Supplementary Fig. 9c (right panel) shows $\langle r^2 \rangle$ *vs* τ in the tracks of 37 separate spots. The linear fit gives an estimate of $D = 0.0088 \pm 0.0026$ μm^2 s^{-1} (mean ± s.d.), consistent with the value deduced by comparison of FRAP data to simulations. The distribution of all intensities for all tracked spots (Supplementary Fig. 9d, 37 spots in 37 cells) shows a peak at 12,600 ± 5,800 counts frame^{-1}. Since the unitary step size due to photobleaching a single GFP molecule is 4,500-6,500 counts s^{-1} (Supplementary Fig. 5c, Supplementary Methods 5) this indicates that the tracked diffusing membrane spots are dimeric in terms of GFP-MotB, consistent with the diffusing unit being a single $MotA_4$:(GFP-MotB)$_2$ stator[16]

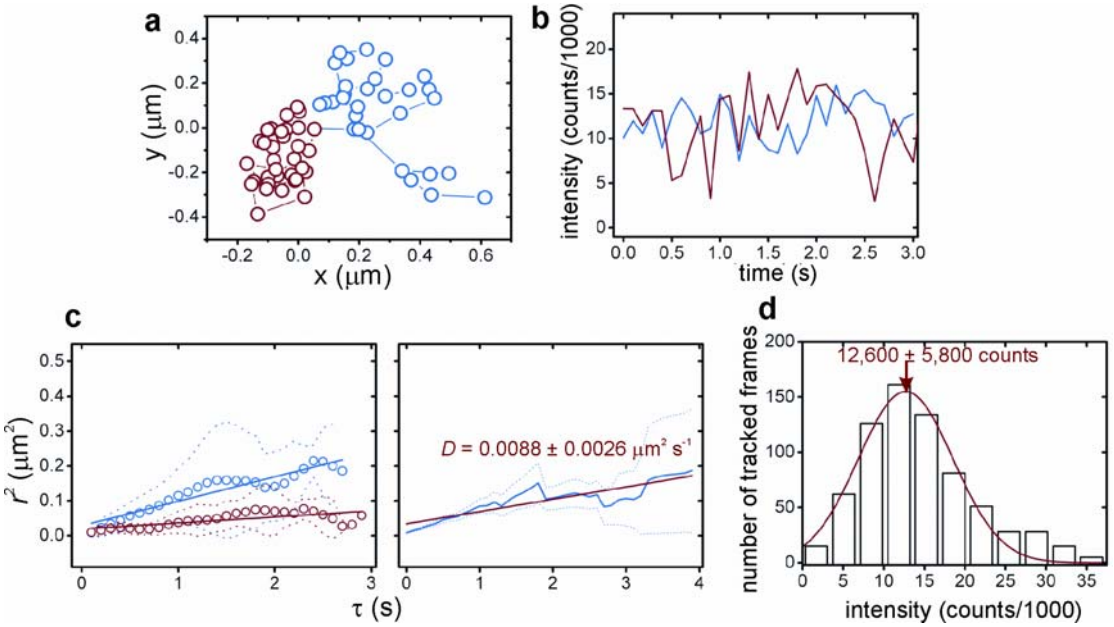

Supplementary Figure 9 Estimating the diffusion coefficient in the membrane by single-particle tracking. **a,** The tracks of the fluorescent spots of Supplementary Video 3 (red) and 4 (blue), from TIRF images of a GFP-MotB cell after pre-bleaching with a focussed laser. Points are Gaussian-weighted centroids of the spot in successive frames, separated by 0.1 s. **b,** Intensity vs time for the same spots as **a**. **c,** Mean-squared displacement (r^2) vs time interval (τ) for the same spots as **a** (left panel mean values are circles, dotted lines the s.d. boundary) with linear fits indicating D values of ~0.004 (red) and ~0.015 (blue) μm^2 s^{-1} and r^2 vs time interval (τ) averaged across all tracked spots (right panel, mean value is the blue solid line, dotted lines the s.e.m. boundary) with linear fit (red line), and calculated diffusion coefficient D indicated. **d,** Distribution of intensities for all tracked spots in the membrane (37 spots from 37 different cells) with Gaussian fit (red line) and centre ± s.d. indicated (arrow).

Supplementary Methods 7

A global model for intensity changes in the motor and membrane. We extended the diffusion model of Supplementary Methods 6 to include GFP photobleaching, and stator exchange between diffusing GFP-MotB and the motor. This model allows us to estimate the rate of exchange with the motor; to verify the methods that we have used to compute the number of GFP molecules per motor (Fig. 2, Supplementary methods 3); and to verify our interpretations of the TIRF photobleach traces (Fig. 2) and FRAP and FLIP data (Fig. 3). The model was implemented in MATLAB as follows:

1. Diffusion of stator units, each containing 2 MotB molecules[16], was simulated as before (Supplementary Methods 6), assuming a total of ~200 GFP-MotB molecules randomly dispersed in the cell membrane and a diffusion coefficient $D = 0.008\ \mu m^2\ s^{-1}$ (values based on experimental estimates).
2. A motor was located centrally on the 'lower' surface of the cylinder (defined as that closest to the TIRF excitation field) as was typical of the experimental assays, initially containing 11 stator units (based on experimental estimate, Supplementary Fig. 5c).

The exchange process was modelled by the standard diffusion-capture method[37]. In every time interval Δt each stator unit attached to the motor either disassociated from the motor or remained bound according to a predefined rate k_d (a free parameter in the program later optimized to actual experimental data): if the unbinding probability, $k_d \Delta t$, was greater than a pseudo-random number in the range 0-1 the unit dissociated, otherwise it remained bound. A small circular region of radius 100 nm centred on the motor was defined as the motor capture zone i.e. a radius ~4 times larger than that of the motor itself (~25 nm). Any free membrane stator units found in this area were polled as above against either binding to the motor or remaining free, according to a predefined rate k_a. We defined $k_a = k_d\ exp(\ f(11-N_s)\ )$, where N_s is the number of stators in the motor at the moment of polling and f a number (we used f = 5) tuning the strength of the exponential factor. This formula ensures that $k_a = k_d$ when $N_s = 11$, and leads to a stable equilibrium number of stators per motor close to the experimentally estimated number. The physical model is that the binding rate is reduced as available binding sites on the motor are occupied and enhanced when there are plenty of empty sites on the motor. We monitor the position of each stator at each time point as well as the bleach state of its GFP molecules and whether it is free or motor-bound.

3. On top of the main code two sub-routines were added, one responsible for bleaching the GFP-MotB in a pre-defined area and the other for predicting, as before (Supplementary Methods 6), the observed fluorescence intensity within a $0.4 \times 0.4\ \mu m^2$ region of interest centred on the motor. For simulations of FLIP and FRAP the bleaching areas were tried in the range 1-2 μm^2 to reflect the size of the focussed laser spot (the largest area tried bleaching ~50% of the total membrane GFP-MotB content in the cell), centred either on the motor (FRAP) or displaced ~1 μm from the motor (FLIP). We assumed that the initial focussed laser spot irreversibly photobleaches a similar quantity of GFP molecules in this area as per the first experimental post-bleach timepoint, on both the lower and upper membranes. For simulations of continuous TIRF bleaching two different bleaching areas were tried; either $\sim 0.6 \times 3.0\ \mu m^2$ centred on the motor (the "TIRF bleach-zone", close to that expected for an excitation field of depth ~100 nm) or the entire lower half of the cell surface (the "extended bleach-zone", modelling

possible scattering of the illuminating light beyond the TIRF field). In each time-step, each un-bleached molecule in the bleach-zone was deemed to have bleached if the probability, $\Delta t/t_0$ (where $t_0 = 40$ s, the experimentally estimated bleach time), was greater than a pseudo-random number in the range 0-1; otherwise it remained un-bleached.

Estimating dissociation rates by simulating FRAP and FLIP experiments. The extended model was simulated with values of k_d equal to 0.01, 0.02, 0.03, 0.04, 0.05, 0.06, 0.07 and 0.09 s^{-1} and bleach-zones corresponding to FRAP and FLIP experiments. For each value of k_d, mean FRAP and FLIP traces for motor and membrane components were obtained by averaging 500 simulations each lasting 300 s (Supplementary Fig. 10a-d, coloured lines). These simulated data-sets were compared to the experimental data-set as follows. For each simulated value of k_d, the error function…

$$E_k = \left(\Sigma_{ij} \left(W_{ij}^2 \, (S_{kij} - \alpha_{ki} D_{ij})^2 \right)\right)^{1/2}$$

was calculated and minimized with respect to α_{ki}. (D_{ij} are experimental FRAP and FLIP data points with weighting factors W_{ij} inversely proportional to standard deviation and S_{kij} are simulated FRAP and FLIP data points. Subscript $k = 1..8$ indicates values of k_d in siumlations, subscript $i = 1..4$ indicates the experimental condition - FRAP or FLIP of motor or membrane components, and subscript $j = 1..9$ indicates the time points between 1 s and 256 s at which experimental data was obtained and compared to simulated data. The re-normalization factors α_{ki} account for uncertainty in the absolute number of MotB-GFP molecules in each experimental data set ($i = 1..4$), arising from the normalization of the mean intensities in the experimental pre-bleach points to 22 GFP molecules per motor (Supplementary Methods 5), and were necessary to generate acceptable fits between the experimental and simulated data.) Supplementary Fig. 10e shows the minimized values of E_k versus the corresponding value of k_d, indicating that the best fit is found for approximately $k_d = 0.04 \pm 0.02$ s^{-1} (error is the width of the Gaussian fit to the residual in the vicinity of the local minimum).

We also investigated the effects of having more than one motor in the cell. Placing three motors randomly within the original bleach spot resulted in no net change in the steady-state value for number of unbleached stators bound to the motor under observation, but did reduce the net total binding rate for unbleached stators at equivalent timepoints compared to the single-motor system by ~5%; adding more bleached motors into the system marginally increases the effective mixing time for bleached and unbleached stators in the membrane.

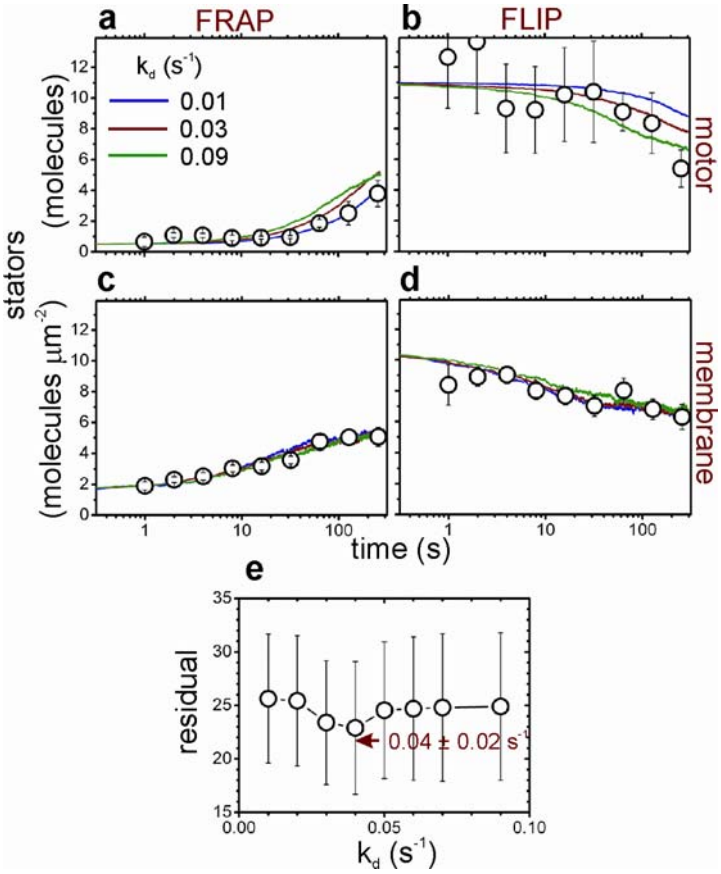

Supplementary Figure 10 Simulations for FRAP and FLIP. Predictions for the FRAP experiment on the motor and membrane components (**a,c**), and similarly for FLIP (**b,d**) at different k_d (showing only three values for clarity). The experimental data, scaled by the re-normalization coefficients α_{4i} that gave the best fit for $k_d = 0.04\ s^{-1}$, are overlaid (white circles, s.d error bars). $\alpha_{4i} = 0.88$ (**a**), 1.28 (**b**), 0.80 (**c**) and 1.00 (**d**). **e,** The minimized error function versus k_d (s.d. error bars).

Testing the fluorophore counting method. We simulated continuous TIRF bleach experiments using value of $k_d = 0.04\ s^{-1}$. To test the accuracy of the unitary step detection algorithm we generated 20 individual simulated bleach traces with a Δt of 100 ms (i.e. 10 Hz sampling) for each of the TIRF and extended bleach-zones (Supplementary Fig. 11a, f). To reflect the experimental protocol we re-sampled each trace at 1 Hz (Supplementary Fig. 11b, g), added Gaussian noise with a width in the range 0.125 to 8.0 times the single simulated GFP photobleach step (i.e. an effective signal-to-noise ratio over the same range, Supplementary Fig. 11e, j) and filtered the trace using the C-K algorithm (Supplementary Fig. 11c, h). We then applied the unitary step detection algorithm used for experimental data (Fig. 2d) to the filtered, simulated traces, obtaining an estimate of the unitary step size for each trace (Supplementary Fig. 11d, i). The mean unitary step size gives an estimate of the accuracy of the detection algorithm as a function of signal-to-noise ratio (Supplementary Fig. 11e, j). Several conclusions emerged from these simulations:

(i) The detection accuracy (the normalized standard deviation of the mean estimate for unitary step size) in a signal-to-noise regime similar to that for experimental data (~1) is ~15%.
(ii) Brief upward steps in motor intensity can be seen in the unmodified 10 Hz simulations, however many of these can no longer be observed when re-sampled at 1 Hz. Further addition of noise and application of the filter remove yet more of these upward steps, so that what remains is more a reflection of downward steps with longer inter-step dwell intervals.
(iii) The frequency of upward steps in the unmodified 10 Hz simulations is less for the extended bleach-zone than for the TIRF bleach-zone.

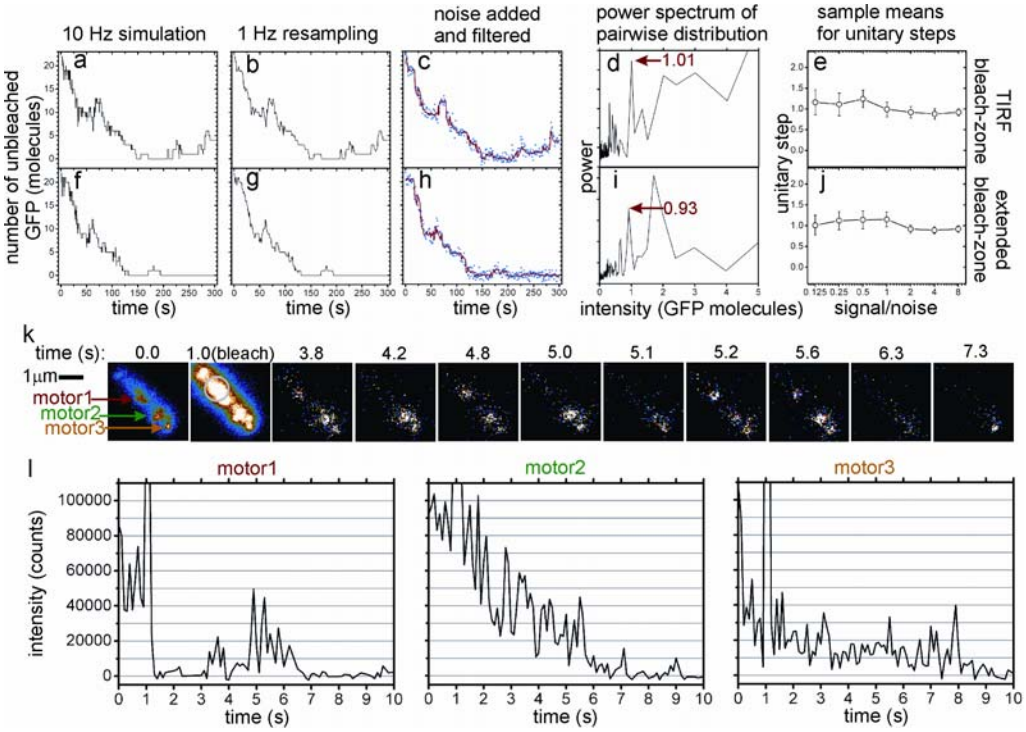

Supplementary Figure 11 Simulations for continuous TIRF bleaching. Simulations are shown using a TIRF bleach-zone (**a-e**), as well as an extended bleach-zone (**f-j**) to illustrate the effects of possible scattering of the illuminating light beyond the TIRF field. Raw 10 Hz simulations (**a,f**); resampled 1 Hz traces (**b,g**) and resampled 1 Hz traces with noise added (**c,h**, blue, filtered output red). **d,i** power spectra (arbitrary power scale) of the pairwise intensity displacement histograms corresponding to filtered traces of (**c,h**) with the positions of the predicted unitary step indicated (red arrow). **e,j** Variation of the predicted unitary steps with different levels of added noise (20 simulations in each dataset, s.d. error bars). **k,** TIRF images of sample stuck GFP-MotB cell pre-bleached using a focussed-laser spot (Supplementary Methods 4). The positions of three motors are indicated (arrows). **l,** The corresponding motor-only intensity traces of the motors indicated in (**k**).

A combination of (ii) and (iii) above is consistent with our observation of comparatively rare detected upward steps in motor intensity when applying our normal 1 Hz sampling experimental protocol. To further test this explanation we applied the modified pre-bleach experimental protocol as per Supplementary Methods 4 (i.e. TIRF frame-rate 10 Hz, pre-bleaching with a focussed laser spot for ~2 s). This photobleached much of the membrane GFP component and therefore increased our effective signal-to-noise ratio for detection of single GFP molecule photobleach events at the motor. Supplementary Fig. 11k shows raw images for such a cell, with Supplementary Fig. 11l the corresponding motor intensities. Upward intensity fluctuations can be seen, similar to those predicted from the simulations, much faster than would be expected from a "GFP-blinking" effect[20] at these relatively low excitation intensities, since this particular enhanced GFP mutant (S65T) has a high probability for being in the emissive state at intensities <1.5 kW cm^{-2} (ref. 38).

Supplementary Methods 8

Slow fluorescence recovery after whole-cell photobleaching. We sampled images continuously for 300 s at 1 Hz, resulting in >90% photobleaching within range of the TIRF field. For completeness, we also performed widefield epifluorescence photobleaching for a further 300 s to complete photobleaching of the entire cell. We saw only minor differences between these two conditions, consistent with the expectation that the majority of GFP-MotB molecules in the cell will diffuse through the TIRF region and be bleached during the 300 s TIRF exposure. We observed recovery in TIRF using the same protocol as focussed FRAP and FLIP experiments (Supplementary Methods 4), at subsequent time intervals up to 90 min. We performed bleaches either in chloramphenicol to suppress new protein synthesis or in motility buffer with or without nutrients (10% tryptone broth). Bleached fluorescent motor spots recovered with their original position and intensity profile (Supplementary Fig. 12a). Whole-cell bleaches in chloramphenicol resulted in recovery levels of ~7% with a 1/e time of ~22 min (Supplementary Fig. 12b, left), close to the measured maturation time for GFP *in vivo*[7]. This implies that a similar percentage of GFP may be non-photoactive in our experimental TIRF photobleaches and thus that the estimate for number of photoactive GFP-MotB molecules at a motor of ~22 from fluorophore counting may be an underestimate of the total number of GFP-MotB by ~1-2 molecules. Permanently inactive GFP molecules may increase the magnitude of the underestimation by a similar number.

Recovery was greater in motility medium lacking chloramphenicol and greater still with added nutrient (Supplementary Fig. 12b, right). We attributed the differences to synthesis of fresh GFP-MotB during recovery.

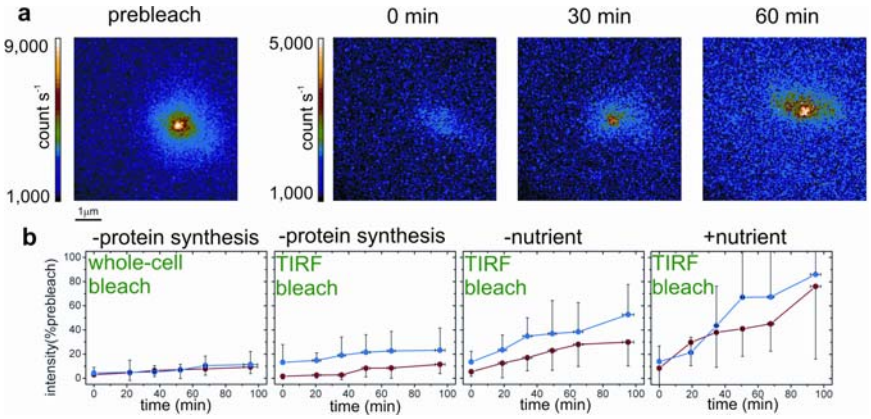

Supplementary Figure 12 Slow recovery after whole-cell photobleaching. Example of TIRF-FRAP on a freely tethered GFP-MotB cell. **a,** TIRF image before photobleach (left panel) and 0, 30 and 60 min subsequently. Note the different intensity scales. **b,** Fluorescence recovery as a percentage of initial pre-bleach intensity. From left to right: whole-cell bleach in chloramphenicol, TIRF-bleach in chloramphenicol, TIRF-bleach in motility buffer and TIRF-bleach in motility buffer plus 10% tryptone buffer. Motor (red) and total background (blue) components are shown. Errors bars at one s.d., 4 cells in each dataset.

Supplementary Methods 9

Determining the extent of anisotropy for motor GFP-MotB molecules. To test for fluorescence anisotropy due to restricted rotation of GFP-MotB when bound to a motor, which might compromise our counting estimate by separating GFP molecules in a single motor into distinct sub-sets according to orientation, we modified our original microscope design (Supplementary Fig. 7a) to generate two orthogonally polarized, independently addressable epifluorescene paths. We used epifluorescence as opposed to TIRF because the polarization state in epifluorescence is better preserved as it passes into the sample from the objective lens; for TIRF this is only true for the S-polarized component whereas the P-polarized field "cartwheels" along the surface with a spatial periodicity of $\lambda/(n_1 \sin\theta)$ (ref. 34). We removed lens L3 from path 2 and added an equivalent beam expander to path 1 (i.e. consisting of lenses equivalent to L1 and L2). We then moved both L2 equivalents to the on-axis epifluorescence position and adjusted the $\lambda/2$ plate to give equal intensities for paths 1 and 2, adjusting the neutral density filters to give an excitation intensity at the sample ~100 W cm^{-2} for each path.

Denoting the orthogonal polarizations via paths 1 and 2 as P1 and P2 respectively, we alternated excitation between P1 and P2 (ref. 36) by switching shutters Sh1 and Sh2 (shutter bandwidth ~1 kHz) at times 2, 4, 8, 16, 32, 64 and 128 s, while simultaneously recording images of stuck cells at 2 Hz (Supplementary Fig. 13a). The background noise was considerably increased compared to TIRF illumination; nonetheless, we were able to calculate the intensity of a motor spot in the same manner as before. Supplementary Fig. 13b shows mean intensity curves calculated for 20 different motors in the GFP-MotB strain (compared against a similar curve of total intensity using the parental non-GFP strain RP437, 12 cells). If rotation of the GFP fluorophores were significantly restricted on the timescale of the image exposures, 0.5 s, then each switch of excitation polarization would correspond to a switch from observing a subset of fluorophores that were preferentially bleached during the previous interval (because their dipoles were well aligned to the excitation polarization of that interval) to a subset that were not bleached during the previous interval (because their dipoles were badly aligned to the excitation polarization of that interval). This would produce stepwise increases in fluorescence, co-incident with the polarisation switches. The intensity curve of Supplementary Fig. Fig. 13b shows no such increases, indicating that GFP fluorophores in the motor are not significantly rotationally constrained.

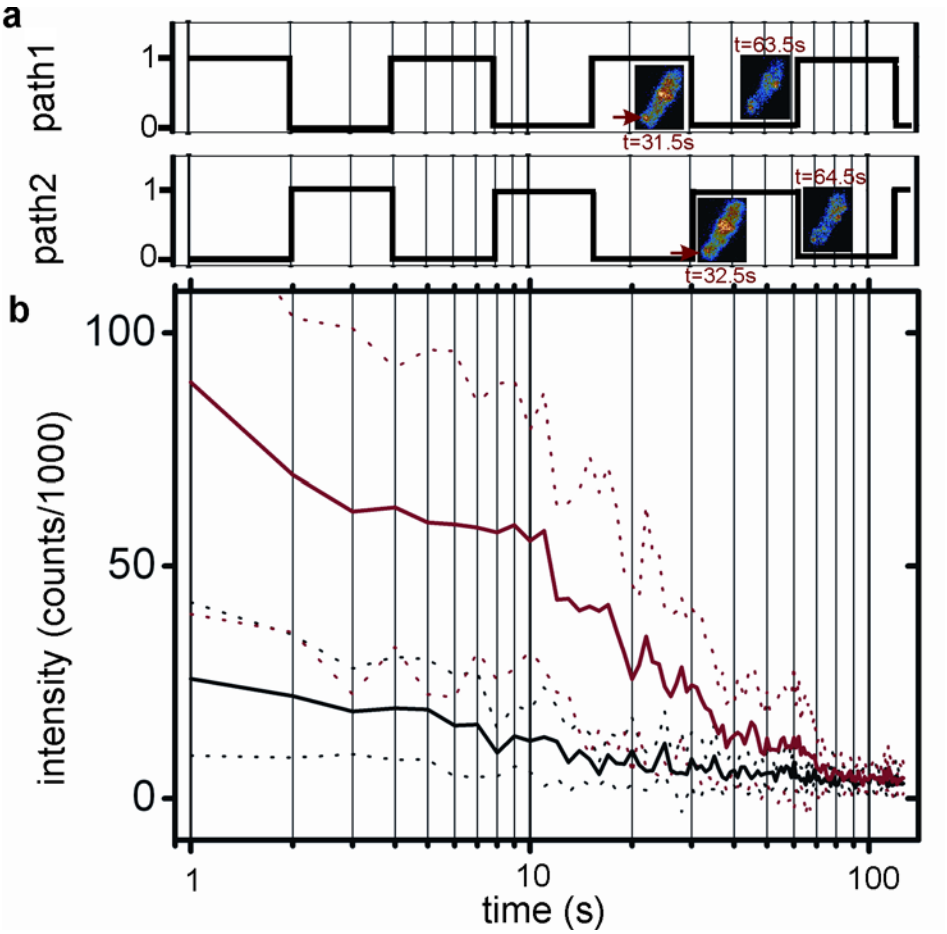

Supplementary Figure 13 Characterizing anisotropy. a, Relative excitation intensities for paths 1 and 2. Images before and after the 32 and 64s switch points are shown for a GFP-MotB cell with the position of the motor under observation indicated (arrow). **b,** Variation of mean intensity (solid lines) with s.d. boundaries (dotted lines) for GFP-MotB cells (red, motor intensity shown, 20 cells) and the parental non-GFP RP437 strain (black, total intensity shown, 12 cells).

Further references:

28. Wadhams G.H., Warren A.V., Martin A.C. & Armitage J.P. Targeting of two signal transduction pathways to different regions of the bacterial cell. *Mol Microbiol.* **50**, 763-770 (2003).
29. Link, A.J., Phillips, D. & Church, G.M. Methods for generating precise deletions and insertions in the genome of wild-type *Escherichia coli*: application to open reading frame characterization. *J. Bacteriol.* **179**, 6228-37 (1997).
30. Berg, H.C. & Turner, L. Torque generated by the flagellar motor of *Escherichia coli*. *Biophys. J.* **65**, 2201-16 (1993).
31. Thompson R.E., Larson D.R. & Webb, W.W. Precise Nanometer Localization Analysis for Individual Fluorescent Probes. *Biophys. J.* **82**, 2775–2783 (2002).
32. Smith D.A. A quantitative method for the detection of edges in noisy time-series. *Philos. Trans. R. Soc. Lond. B Biol. Sci.* **353**, 1969-81 (1998).
33. Chung S.H. & Kennedy R.A. Coupled Markov chain model: characterization of membrane channel currents with multiple conductance sublevels as partially coupled elementary pores. *Math Biosci*. **133**, 111-37 (1996).
34. Kuo, S. C., Gelles, J., Steuer, E. & Sheetz, M. P. A model for kinesin movement from nanometer-level movements of kinesin and cytoplasmic dynein and force measurements. *J. Cell Sci.* **14** (suppl.), 135-138 (1991).
35. Axelrod, D., Thompson, N.L. & Burghardt, T.P. Total internal reflection fluorescent microscopy. *J. Microsc.* **129,** 19-28 (1983).
36. Schuetz G, Schindler H. & Schmidt T. Imaging single-molecule dichroism. *Optics Lett.* **22**, 651-653 (1997).
37. Berg H.C. *In* Random walks in biology. *Princeton University Press* **Ed.4** 37-47 (1993).
38. Garcia-Parajo M.F., Segers-Nolten G. M. J., Veerman J.-A., Greve J., & van Hulst N. F. Real-time light-driven dynamics of the fluorescence emission in single green fluorescent protein molecules. *Proc Natl Acad Sci U S A.* **97**, 7237–7242 (2000).